Tidal Flexure, Ice Velocities, and Ablation Rates of Petermann Gletscher, Greenland

Eri(Rignot

Jet Propulsion laboratory, California Institute of Technology, Pasadena 91]09, California, U.S.A.

ABSTRACT Over the floating section of a tide-water glacier, single radar interferograms are difficult to use because the long-term steady motion of the ice is intermixed with the tidal vertical motion of the glacier. With multiple interferograms, it is however possible to isolate the tidal signal and subsequently remove it from the single interferograms to estimate the ice velocities. The technique is applied to ERS-1 synthetic-aperture radar (SAR) images of Petermann Gletscher, north Greenland. The precision of the tidal measurements is 1-2 mm d^{-1}. Ice velocities are known within 1 m a^l The tidal measurements agree well with model predictions from a fixed elastic beam with an elasti C damping factor Of 0.47 km^{-1}, By localizing the maximum of the bending stress along each image line, the hinge-line is mapped with a precision of 20 m. The interferometric hinge-line may be used as a reference for detecting future meter-scale changes in ice thickness of the glacier tongue. At the glacier center-line, the hinge-line shifts 2 km along-flow over a 500-m transverse distance, initiating a longitudinal rupture of the ice tongue. Transverse ruptures appear at regular intervals 20-40 km down-stream as fast-moving ice slabs override slower-lnovi])g portions of the ice tongue. Ice discharge of the ice tongue is calculated using the ice velocities and ice thickness estimates obtained from a digital elevation model of the glacier. The results show a decrease from 10.8 km^3 a^{-1} at the hinge-line to 1.6 km^3 a-1 about 30 km downstream from the hinge-line, which is equivalent to a glacier thinning rate of 13.6-m a-1. Closer to the ice-front, the glacier thinning rate is 2.3 m a^{-1}. Surface ablation of about 1-3 m a-' may explain glacier thinning near the ice-front but cannot explain the enhanced thinning rate near the hinge-line, which must be due to basal ablation. Basal ablation is the dominant process of mass release from Petermann Gletscher. Basal and surface ablation together melt 95% of the mass discharged across the hinge-line before it reaches the glacier front.

INTRODUCTION

Calving glaciers play an essential role in the dynamics and mass balance of the Greenland Ice Sheet, and even more in the case of the Antarctica Ice Sheet where ice shelves and ice tongues develop extensively (Holdsworth, 1977; Hindmarsh, 1993; Vaughan and Doake, 1 996). of particular interest for studies of the stability of these glaciers is the region at the junction between slow moving ice from the inland ice where no tidal displacements occur and the faster moving ice from the ice tongue or ice shelf where tidal forcing introduces a cyclic vertical flexure of the ice surface. The point where the ice separates from the glacier bed, the grounding line, is important to locate precisely b ecause it provides a basis for monitoring changes in ice-thickness or sea-level induced by climate shift (Smith, 1991).

Tidal ice-shelf flexure may be measured by tiltmeters (Smith, 1991) or precise GP'S kinematic surveys (Vaughan, 1 994). Locating the grounding line is more difficult by traditional standards and there are no systematic means to map its position from a remote sensing instrument. Goldstein et al. (1 993) detected tidal motion of the Rutford ice stream with ERS-1 interferometric radar data and deduced the grounding line at a resolution of 0.5 km. Ice velocities, or the long-term steady motion of the ice, could not be estimated from the SAR interferogram because the component of horizontal motion is inherently mixed with the tidal vertical motion of the ice surface. Hartl et al. (1994) however demonstrated the tidal signal could be separated from the ice velocities by differencing the signal obtained in two consecutive interferograms.

The same technique is applied here, by which the tidal signal is separated from the steady motion of the ice using two interferograms. The mapping of the hinging or bending zone of the ice is improved by an order of magnitude bc.cause the measurements are no longer perturbed by the longitudinal strain rates of the long-term steady motion of the ice. By re-introducing the tidal signal into the radar interferograms and assu ming an elastic de-

formation of the ice tongue, it is also possible to subsequently retrieve the ice velocities of the floating section of the glacier. The technique is demonstrated in the case of Petermann Gletscher, a major outlet glacier of northern Greenland, which develops into an extensive ice tongue confined within a fjord. Numerous rock outcrops are present to provide a reliable, fixed reference for estimating the interferometric baselines and studying glacial motion. Data coverage by ERS-1 SAR of that part of Greenland is excellent. In addition, S. Ekholm et al., KMS (Kort and Matrikelstyrelsen) produced a very precise topographic map of the region, which includes all glacier areas. Several other studies win-c conducted 011 this glacier in recent months. Joughin et al. (1995) studied the mass balance of Petermann Gletscher using interferometric measurements and ice thickness data near the equilibrium line altitude. Jezek et al. (1995) studied basal processes 011 several Greenland outlet glaciers, including Petermann Gletscher, and stressed the importance of basal ablation processes in the overall mass budget of Petermann Gletscher. The present study focuses on the ice flow dynamics of the glacier ice tongue using ERS-1 SAR interferometry data with implications for other ice tongues and ice shelves.

STUDY AREA

Petermann Gletscher is located 60° west and 81° north, 011 the north-western flank of the Greenland Ice Sheet. Petermann Gletscher was first documented and examined during the United States 'Polaris' expedition under C.F. Hall in 1871 (Kollmeyer, 1980). It is one of the few Arctic glaciers which develops into an extensive ice tongue. Large portions (>50 kin) of its outer front are floating, and the terminus is only 3 to 4 m above sea level (Higgins, 1991). Calf ice is produced by occasional disintegration of its terminus, which yields tabular icebergs 30-50 In thick, up to 10 km x 12 km in size (Dunbar, 1978; Kollmeyer, 1980). The glacier width is 30 km when it merges with the inland ice, narrowing gradually northward over its 100 km length to reach 12 km at the terminus. Surface altitude decreases from 600 m

at the inland ice margin to only 25-35 m at Kap Coppinger (Higgins, 1991). Petermann Gletscher has the highest measured velocity of north Greenland glaciers, about 0.95 km a^{-1} at the ice front (Higgins, 1991).

This study utilized 3 consecutive passes of ERS-1 SAR acquired on February 25, 28 and March 2, 1992, during orbit 3205, 3248 and 3291 of the satellite. Each image is a 100 km x 100 km frame, with a 20-m pixel spacing on the ground after averaging of 5 pixel elements in the azimuth (along-track) direction. The upper 72 km of the radar amplitude image are shown in Figure 1. North is on top, with ERS- 1 flying from east to west, looking north to its right. Petermann Gletscher runs south-north in between Washington Land to the west and Hall Land to the east. The shear margins of the glacier are very pronounced and extend far southward into the mainland ice. Most of the glacier surface within the fjord is radar-dark indicating a surface poorly reflective of the radar signals. The radar-bright region to the south shows the transition with the percolation facies of the inland ice which are radar-bright because of internal reflections in sub-surface icy inclusions (Rignot, 1 995). Five glaciers descend on the east side from Kane plateau to merge with the main ice stream (Higgins, 1991). The most important one is Porsild Gletscher (Figure 1).

METHODS

1 nterferogram Generation.

Readers interested in a background on radar interferometry may consult Zebker and Gold- stein (] 986), Goldstein et al. (1 988), Gabriel et al. (1989), and Zebker et al. (1994). The basic principles of radar interferometry will not be repeated here.

Two interferograms were formed using image 2 (orbit 3248) as the reference image in both interferometric pairs. The complex amplitude images were c.o-registered with sub-

pixel accuracy, including additional pixel off'sets over fast-moving portions of the ice, and cross-correlated. The phase coherence of the resulting interferometric products, denoted ρ and taking values between O (no coherence) and 1 (perfect temporal coherence), was high ($\rho > 0.8$) over most of the scene, yielding high quality interferometric fringes (Figure 2). Phase unwrapping was performed using Goldstein et al., (1988)'s unwrapping algorithm after smoothing the data using a 2-dimensional spectral filter (Werner, unpublished, 1995). Above the hinging zone, the interferograms exhibited a complex pattern of closely-s])aced fringes **(360°** variations in phase) and phase unwrapping was difficult. Similar patterns were observed on the south-western flank of the Greenland Ice Sheet and attributed to vertical motion of the ice over bumps and II ollows, several meters in height and several kilometers in diameter, created by faster ice sheet flow over the bedrock topography near the ice margin (Rignot et al., 1995; Joughin et al., 1 995). To unwrap the phase values across those regions, the radar data were analyzed at high resolution (5-looks), and phase unwrapping was performed in sub-blocks, subsequently pieced together to maintain the continuity of the phase. A second set of interferometric pairs corresponding to orbit 2904, 2947 and 2990 was also analyzed, but the phase values could not be unwrapped as successfully as for the present set of images.

The baseline separation between the successive positions of the radar antenna was estimated by lcasi-square fitting using 1,400 tie-points selected from a digital elevation model (DEM) of the glacier, 0.005° in latitude spacing and 0.025<' in longitude spacing, provided by S. Ekholm, KMS. The DEM was interpolated, projected into the radar imaging geometry, and registered with the SAR data within 1-2 SAR pixels using one tie-point.

Interferometric Products.

Let us denote by V_x, V_y, V_z the components of the steady motion vector of the ice along the x-, y- and z-axis. The x-axis is in the cross-track direction, pointing north. The y-

axis is in the along-track direction, pointing west. The z-axis is the vertical axis. Under tidal influence, the ice tongue undergoes upward and downward motion along the z-axis of amplitude Z. Here, we use the sign convention that the phase, ϕ, measured by the radar is $\phi z - \frac{4\pi}{\lambda} R$ where R is the range distance between a point and the center of the synthetic aperture, and λ is the radar wavelength (5.66 cm for ERS-1 SAR). The phase difference, $\phi_{12} = \phi_2 - \phi_1$, measured between antenna 1 (orbit 3205) and 2 (**3248**) may be expressed as

$$\phi_{12} = \frac{4\pi}{\lambda}[B_{12\perp}\ \sin(\delta\theta_z) - B_{12\parallel}\ \cos(\delta\theta_z) + \frac{B_{12}^2}{2R}] + \qquad (1)$$
$$\frac{4\pi}{\lambda}[-V_x\ \sin(i) + V_z\ \cos(i)](t_2 - t_1) +$$
$$\frac{4\pi}{\lambda}[Z_2 - Z_1]\cos(i) + \phi_{12}^o$$

B_{12} is the baseline or distance separating antenna 1 and 2, α_{12} is the baseline angle with the horizontal, θ_o is the illumination angle with the horizontal at the center of the scene for a point at reference elevation $z = 0$, θ_z is the illumination angle for a point at elevation z above the geoid, $\delta\theta_z = 0.--00$, $B_{12\perp} = B_{12}\sin(\theta_o + \alpha_{12})$ is the component of the base.lilie perpendicular to the direction of the radar illumination, $B_{12\parallel} = B_{12}\cos(\theta_o + \alpha_{12})$ is the component of the baseline parallel to the direction of the radar illumination, $(t_2 - t_1)$ is the time lag between the two images, and ϕ_{12}^o is the absolute phase offset.

The first line of Eq. (1) is the topography term, which is scaled by the baseline. The second line describes the ice velocity along the radar line of sight caused by tile steady motion of tile ice. The third line corresponds to changes in surface elevation along the radar line of sight caused by the downward motion of the ice under tidal influence. With a second interferogram combining image 2 and 3, we have

$$\phi_{32} = \frac{4\pi}{\lambda}[B_{32\perp}\ \sin(\delta\theta_z) - B_{32\parallel}\ \cos(\delta\theta_z) + \frac{B_{32}^2}{2R}] + \qquad (2)$$
$$\frac{4\pi}{\lambda}[-V_x\ \sin(i) + V_z\ \cos(i)](t_2 - t_3) +$$

6

$$\frac{4\pi}{\lambda} [Z_2 - Z_3] \cos(i) + \phi_{32}^o$$

If 1, 2 and 3 are acquired in sequence and 3 days apart, adding Eq. (1) and (2) eliminates the term of steady motion to yield

$$\phi_{12} + \phi_{32} = \frac{4\pi}{\lambda}[(B_{12 \perp} + B_{32 \perp}) \sin(\delta\theta_z) - \tag{3}$$

$$(B_{12 \parallel} + B_{32 \parallel}) \cos(\delta\theta_z) + \frac{B_{12}^2 + B_{32}^2}{2 R} +$$

$$[2 Z_2 - Z_3 - Z_1] \cos(i)] + \phi_{12}^o - 1 \quad \phi_{32}^o$$

Eq. (3) is similar to Eq. (I), with a perpendicular and parallel baseline equal, respectively, to the sum of the perpendicular and parallel baselines from both interferograms. Using tie-points from the KMS DEM on both rock and ice, but excluding the ice tongue, we estimated the baseline parameters of Eq. **(3)** and eliminated surface topography to obtain

$$\phi_{12,flat} + \phi_{23,flat} \cdot \frac{4\pi}{\lambda}[2 Z_2 - Z_3 - Z_1] \cos(i) \tag{4}$$

which only depends on tidal flexure. The map of tidal displacements, $Z_2 - 0.5 (Z_3 - Z_1)$, is shown in Figure 3.

Model predictions from the elastic beam theory indicate tidal displacements along an elastic beam vary linearly with tidal amplitude. Several experimental studies have shown the elastic beam model matches observations very well (Holdsworth, 1969). Assuming tidal forcing is the same everywhere along the beam (Holdsworth, 1969), and the elastic damping factor does not change with tidal amplitude (Holdsworth, 1977), a difl'emit realization of tidal forcing should exhibit the same pattern of tidal flexure as that given from Eq. (4), scaled by a different tidal amplitude. Under hese assumptions, we may JC'-write Eq. (1), after removal of the topography term, as

$$\phi_{12flat} = \frac{4\pi}{\lambda} [-V_x \sin(i) - i V_z \cos(i)] (t_2 - t_1) + \tag{5}$$

$$\gamma_{12} [\phi_{12,flat} + \phi_{23,flat}] + \phi_{12}^o$$

Eq. **(5)** yields the ice velocities, provided γ_{12} is known.

To determine γ_{12}, one point of known horizontal velocity is needed on the floating part of the glacier. To obtain those control velocities, we tracked trains of crevasses below the hinge-line in ERS-1 images acquired one year apart. The result is $\gamma_{12} = 1.830.2$, with a 50-in a^{-1} rms error in the 11 control points, comparable to the precision of the feature tracking results, The x-velocity, V_x, was deduced from Eq. (5) assuming $V_z = 0$ because the vertical velocity component associated with glacier thinning is negligible compared to tile horizontal motion, and ice flows approximately in the horizontal plane because of the low surface slopes. The x-velocity map was subsequently transformed into an horizontal velocity map by assuming a flow direction parallel to the dotted line shown in Figure 1, which approximates the dynamic center-line of the glacier. The dotted line follows the glacier center-line where indicated by surface crevassing (Figure 1), and the line of maximum velocity in the radar looking direction elsewhere (Figure 2). The results are shown in Figure 4.

Measurement Uncertainties.

The rms error in phase of the radar signal calculated during the estimation of the baseline using several hundred tie-points was 3 for pair 3248 -320.5 (Eq. 1), 0.6 for pair 3248-3291 (Eq. 2) and 7 for the two pairs combined (Eq. 3). These phase errors translate into uncertainties in surface topography of, respectively, 75, 400 and 180 m. The errors are large because the perpendicular base.lilles were short (respectively 58, 2 and 60 m), but an accurate topographic map was already available. In terms of ice motion, the phase errors translate into uncertainties of 4, I and 10 mm d^{-1} of motion, which is two orders of magnitude less than the velocity of the glacier (2000-3000 m d^{-1}) and one order of magnitude less than the tidal amplitude (200-300 mm). As shown in Figure 3, phase errors form large scale features, not correlated with topography, which implies they are not due to baseline uncertainties or errors in the DEM. They are most likely associated with atmospheric propagation delays

8

(Goldstein, 1995).

At the pixel level, the dominant source of error is phase noise, σ_ϕ, given by (Li and Goldstein, 1990; Rodriguez and Martin, 1992)

$$\sigma_\phi = (1 - \rho)^{1/2} \rho^{-1} N^{-1/2} \tag{6}$$

where N is the number of looks, here equal to .5. Over rock, $\rho > 0.85$ (Figure 2) so $\sigma_\phi < 0.2$, which is equivalent to 0.3 mm d^{-1} of motion when σ_ϕ is multiplied by $(4\pi)/\lambda)^{-1}$. Over land ice, ρ varies between 0.5 and 0.8 (Figure 2), yielding σ_ϕ equivalent to 0.3 and] 111111 d-1 of motion. Over the ice tongue, ρ is also about 0.8 (Figure 2). At the hillge-line, $\rho = 0.4$, and σ_ϕ is equivalent to 1.3 mm d^{-1} of motion. In the region where ice flow is strongly convoluted with surface topography, areas where $\rho < 0.25$ were not unwrapped, SC) σ_ϕ corresponds to less than 2 mm d^{-1} of motion. With $N = 80$ looks, pixel spacing is degraded to 80 m and the above error estimates are divided by 4. To map the hinge'-]ine, we used $N = 5$, but for all other applications we used AT = 80 since spatial resolution was not a critical factor.

RESULTS

Tidal Flexure.

The pattern of tidal flexure (Figure 3) delineates the portion of the glacier that is afloat. Nearly the entire section of the glacier undergoes tidal motion. Tidal displacements are riot uniform and exhibit three-dimensional structures. 'J'ids] flexure is maximum at the glacier center-line and decreases toward the glacier margins where restraints by the rock margins must limit the amplitude of the tidal displacement. 'J'ids] flexure increases in the along-flow direction to peak at about 6 km from the edge of the hinging zone. On tile eastern side of the glacier, near where Porsild Gletscher merges with the main stream of Petermann Gletscher, the rate of maximum increase in tidal flexure is twice smaller and the direction

of increase is 45° off compared to the direction of increase in the western section of the ice tongue. Phase unwrapping failed on Porsild Gletscher, but the glacier is likely to undergo tidal motion as well. The complex pattern of tidal motion observed on the eastern margin is therefore probably associated with the interplay of the hinging zones from both glaciers.

The tidal profile extracted along the western half of the ice tongue (Figure 1) was compared with model predictions from an elastic beam of infinite length, with one end rigidly clamped on bedrock (Holdsworth, 1977). The predicted tidal amplitude is

$$Z = Z_L [1 - e^{-\beta x} (\cos (\beta x) + \sin (\beta x))] \tag{7}$$

where β is the elastic damping factor given by

$$\beta^4 = 3 \rho_w g (1 - \nu^2) E^{-1} h^{-3} \tag{8}$$

E is the elastic modulus of ice, $\rho_w = 1030 \, \mathrm{kg \, m^{-3}}$ is the density of sea-water, $g = 9.81 \, \mathrm{m \, s^{-2}}$ is the acceleration of gravity, $\nu = 0.3$ is the poisson coefficient for ice, and h is the glacier thickness. The best fit was obtained for $\beta = 4.7 \, 10^{-4} \mathrm{m}^{-1}$, with a rms fit error of 0.8 mm (Figure 5). Judged from the low rms error and the high number of points used in the comparison, the model predictions fit the measurements very well. Residual errors are concentrated beyond the point of maximum tidal deflection where the model overpredicts the tidal displacements.

Using Eq. (8) and $E = 0.88$ GPa (Vaughan, 1995), we calculate an ice thickness of 800 m at the hinge-line. The actual thickness is 540 m. Using Eq. (8), we find $E = 3.6$ GPa in order to obtain $\beta = 4.7 \, 10^{-4} \mathrm{m}^{-1}$. We conclude our data do not support the contention that an elastic modulus of the ice of about 0.88 GPa explains most observations of tidal flexure at ice shelf or ice tongue margins (Vaughan, 1995). Considerable spread exists in the values of the elastic modulus of the ice obtained from fitting of an elastic beam model through observations of tidal flexure.

10

Hinge-line.

The tidal displacements were utilized to calculate the bending strain rate, $\dot{\epsilon}_{xx} = \partial^2 Z/\partial x^2$, and the bending stress of the ice surface, $\sigma_{xx} = E\dot{\epsilon}_{xx}(1 - \nu^2)$-], which is maximum at the hinge-line, for $x = 0$, (Holdsworth, 1977). For -d 0.2 m deflection of a 540-m thick ice beam, we calculated a maximum σ_{xx} of 80 kPa. Locating the maximum bending stress of the ice however increases the noise level of the data because of the second order derivatives. Instead, we located the local minimum tidal displacement (Figure 5) and mapped the hinge-line accordingly across nearly the entire glacier width. The results are shown in Figure 3. Based on the noise level of the tidal signal, the position of the hinge-line is known within 1 pixel or 20 m. The achieved precision is more than one order of magnitude superior to that quoted in the preliminary assessment by Goldstein et al. (1993) who utilized a single interferogram. One exception is the glacier center-line where the hinge-line shifts along-flow by 2 km over an across-flow distance of about 500 m. The tidal profiles in this area do not exhibit a sharp minimal deflection compared to that in other portions of the ice tongue so the determination of the hinge-line is less precise, probably of the order of several pixels (50-100 m) rather than one pixel. No discontinuity in surface strain rate is detected in the transition arm, but the results suggest tidal motion triggers glacier rupture. Surface rupture is clearly visible a few km downstream of the hinge-line (Figure 1), exactly aligned with the zone of abrupt longitudinal displacement of the hinge-line.

Ice Velocities.

Ice velocities vary from 400 m a^{-1} at about 900 m elevation to 1100 m a-' at the hinge-line, decreasing thereafter to about 900 m a^{-1} toward the edge of the scene (Figure G). Removal of the tidal signal clearly reduced the variations in ice velocity across the hinge-line (Figure 6), yielding a more reasonable velocity profile. Vertical motion of the ice over bumps and hollows in surface topography are also considerably reduce.d on the ice tongue

compared to that on the grounded ice (Figure 6). This result is expected since the grounded ice surface topography reflects variations in bedrock topography, whereas the floating-ice topography is usually nearly level. Longitudinal strain rates are also lower on the ice tongue than on the grounded inland ice, which is consistent with the expected reduction in basal flow-resistance as the glacier goes afloat.

In several places, large discontinuities in surface strain rates are observed (Figure 4). Along the center-line, the eastern slab of the ice tongue moves at about 30-50 m a^{-1} faster than the western slab. At about 20 km from the hinge-line, where the velocity difference between the two slabs is about 50 m a', the velocity of the eastern slab abruptly decreases by 40 m a'. The discontinuity in velocity and apparent surface rupture do not correspond to an extension of the eastern slat) but to an overriding of its northern section causal by faster motion from the south. Another 20 km downstream, overridding occurs 011 the western slat) with a discontinuity in velocity also of about 40 m a^{-1}. The discontinuity in strain rate along the center-line is no longer visible, meaning the two ice slabs move at comparable speeds.

Downstream of the hinge-line, the ice tongue must be ruptured across its entire thickness because of the large difference in velocity between the two ice slabs. The eastern and western slabs must undergo different levels of flow resistance at the rock margins, and must also friction along the center-line. Once sufficient strain has accumulated along the center-line, the glacier ruptures and the ice velocities re-adjust. Combined with longitudinal glacier fracturing at the hinging zone which creates a zone of weakness which is advected downstream, the transverse rupture patterns seem to form the basis for the formation of the 10 km x 10 km tabular icebergs occasionally seen to emerge from Petermann Gletscher into Hall Basin.

Ice Discharge.

Over the floating section of the ice, we estimated the glacier ice discharge and its along-flow gradient. Ice thickness was estimated from the KMS DEM assuming ice floatation. Ice sounding radar data collected by an airborne instrument from the University of Kansas (Gogineni, unpublished data) along the glacier center-line showed an excellent agreement with the DEM-derived ice thicknesses. For instance, at the hinge-line, the DEM indicates an average elevation of 68 ±6 m, therefore nearly level, as would be expected if the glacier were fully afloat. The ice thickness computed to balance buoyancy forces from scv-water is 540 ±48 m. Ice sounding radar collected along the white line in Figure 1 indicate a glacier thickness of about 560 m. Comparisons performed elsewhere along the glacier center-line indicate a similar level of agreement, about 10-20(% of the ice thickness.

The KMS DEM were utilized to compute the average ice thicknesses of profiles taken along the y-axis, and combined with the x-axis ice velocities (Eq. (5)) and the width of the profile along the y-axis to estimate ice discharge. Because basal velocity of floating ice must equal its surface velocity, the simple multiplication of the average thickness, average velocity, and width of the glacier should yield good estimates of the ice flux, ice thickness being the]Cast-we]] known parameter, Portions of the glacier margins where no interferometric data were available were not utilized so ice discharge is underestimated, yet the error should be of second order magnitude since ice velocity decreases very rapidly in the narrow shear margins of the glacier.

The estimated ice fluxes are plotted in Figure 7 as a function of the along-flow longitudinal distance from the hinge-line. The data exhibit a large decrease in ice discharge in the first 30 km of glacial flow from $10.8\,\text{km}^3\,\text{a}^{-1}$ at the hinge'-li~lc to $1.7\,\text{km}^3\,\text{a}^1$ about 30 km from the hinge-line. Closer to the ice front, the along-flow gradient in ice discharge is lower. Calf-ice production was estimated to be about $0.46\ \text{km}^3\ \text{a}^1$ at the ice front by Higgins (1991).

DISCUSSION

The hinge-line of Petermann Gletscher may move back and forth with the ocean tide depending on the geometry of the hinge zone (Holdsworth, 1977), From the KMS DEM, the glacier slope at the center of the. glacier averages 0.8% at the hinge-line, 1 % 4 km above, and 0.2% 4 km below. If the tidal range is smaller than 20 cm, which may be the norm for ice tongues developing in the Arctic (Holdsworth, 1977), and assuming the glacier surface slope follows the bedrock slope, tidal influence should not displace the hinge-line by more than one pixel Spat.illg 01 20 111. Assuming the hinge-line remains stable within 20 m, an example 12(1 m or 6 pixels lo]lg-term shift in position of the Hillgc-line would indicate a 1-m change in ice thickness of Petermann Gletscher. Using the interferom etrically-deri ved hinge-line should therefore provide a fine reference for detecting future subtle changes in glacier conditions, even though surface slopes are moderate. For comparison, detecting ln~tc'r-scale changes in ice thickness from the differencing of multj-date interferometrically-derived topographic maps would be difficult to achieve (Rodriguez and Martin, 1992).

The most striking observation remains the pronounced along-flow decrease in ice discharge and ice thickness of the ice tongue. Using multi-date **SAR** imagery, feature tracking, and ice sounding radar thickness data, Jezek et al. (1995) argued that a significant amount of ice must be removed from the ice tongue by basal ablation. Here, we are able to quantify the ice removal by ablation processes and provide further support for their conclusion that basal ablation plays a dominant role in the ice discharge from Petermann Gletscher.

The decrease in ice discharge in the first 30 km averages -0.28 km^2 a^{-1}. Most of the decrease is due to a 77% reduction in glacier thickness because ice velocity is only reduced by 5% and glacier width is only reduced by 7%. The decrease in ice thickness is equivalent to a glacier thinning rate of 13.6 m a–1 assuming a mean ice velocity of 1000 m a^{-1}, Closer to the ice front, the equivalent glacier thinning rate is 2.3 m^{-1} in the last 40 km, close to the 2.7-m 1

14

estimate of Higgins in the last 17 km of glacier flow, Higgins interpreted glacier thinning as resulting from surface ablation, quoting surface ablation rates in north Greenland of about 1-311) a^{-1}. Near the liillgt'-lillc,l~of~'ever, surface ablation cannot explain the magnitude of the thinning rate, which must be attributed to basal ablation. Basal melting is largest near the hinge-line and decreases down-flow. Assuming the linear trend in ice discharge in the last **40** km of glacial flow is due to surface ablation (Figure 7), basal ablation discharges about 8.3 km^3 a^{-1} below the hinge-line, while surface ablation must remove only 2.5 km^3 a^{-1}. Surface and basal ablation combined account for over 95% of the mass release across the hinge-line before it reaches the ice front.

The contribution of mass release from basal melting is t Here.fore considerable, Basal ablation is the dominant process of mass release from the hinge-line of Petermann Gletscher. Large errors in its mass balance budget would result from assuming that mass release only proceeds through surface ablation and calf-ice production. The results stresses the importance of including basal melting in mass balance studies of tide-water glacier developing into an ice tongue. Ice tongues similar to that of Petermann Gletscher may not develop extensively in the Arctic, which implies that current estimates of the mass balance of the Greenland Ice Sheet may not be significantly off as a result of neglecting the contribution from basal melting. In Antarctica, where far more glaciers develop into ice tongues and ice shelves, including the role of basal ablation processes should be of much greater relevance. This study shows radar interferometry is a powerful tool for determining the precise location of the hinge-line and for measuring ice discharge at the hinge-line rather than at the ice front.

Here, the glacier topography was a-priori known from an existing KMS DEM. Radar interferometry may however also be used to obtain surface topography. Large perpendicular baselines would be needed to obtain a precision in topographic mapping (1-2 m vertical) sufficient to obtain reliable ice thickness estimates. In an ideal situation, ice motion would he

determined using two interferograms with nearly-zero perpendicular baselines, and surface topography would be inferred using a third interferogram with a large baseline.

CONCLUSIONS

ERS-1 SAR data were utilized to measure the tidal flexure of the ice tongue of Petermann Gletscher with a precision of about 2 mm d~ and to map the hinge-line of the glacier with a precision of 20 m, across nearly its entire width. The interferometric hinge-line should provide a reference for monitoring future meter-scale long-term changes in ice thickness of Petermann Gletscher. Ice velocities estimated on both the grounded and floating portions of the ice revealed ice discharge decreases rapidly downstream from the hinge-line, at a rate which cannot be explained by surface ablation, and which must be caused by basal melting. Similar studies conducted on other ice tongues developing in the Arctic as well as on the extensive Antarctic ice shelves should bring significant new insights into glaciological processes occurring at the boundary between inland and floating ice

REFERENCES

Dunbar, M. 1978. Petermann Gletscher: Possible source of a tabular iceberg off the coast of Newfoundland. *J. Glaciol.*, 20(84), 595 597.

Gabriel, **A. K.**, R.M. Goldstein and H.A. Zebker. 1989. Mapping small elevation changes over large areas: differential radar interferometry. *J. Geophys. Res.*, 94(117), 9183-9191.

Goldstein, R.M., 11 .A. Zebker and C.L. Werner. 1988. Satellite radar interferometry: two-dimensional phase unwrapping. *Radio Sci.*, 23(4), 713-720.

Goldstein, R.M. 1995. Atmospheric limitations to repeat-track radar interferometry. *Geophys. Res. Lett.*, 22(1 8), 251 7-2520.

Goldstein, R.M., II. Engelhardt, B. Kamb and R.M. Frolich. 1993, Satellite radar interferometry for monitoring ice sheet motion: application to an Antarctic ice stream. *Science*, **262(5139), 1525- 1530.**

Hartl, P., K.H. 'l'hiel, X. Wu, C. Doake and J. Sievers. 1994. Application of SAR interferometry with ERS-1 in the Antarctic. *Earth Observation Quaterly* 43, ESA Pub., i- 4.

Higgins, A. 1990. North Greenland glacier velocities and calf ice production. *Polar forschung*, GO(l), 1- 23.

Hindmarsh, R. C.A. 1993. Modeling the dynamics of ice sheets. *Progress Phys. Geog.* **17** (4), 391-412.

Holdsworth, G. 1969. Flexure of a floating ice tongue. *J. Glaciol.*, 8(54), 385 397.

Holdsworth, G. 1977. Tidal interaction with ice shelves. *Ann. Geophys.*, 33(1 /2), 133-146.

Jezek, K., 1'. Gogineni, and E. Rignot. 1995. Radio echo sounding of outlet glaciers, western Greenland, *EOS Trans.* Fall Meeting 1995, 1111 D-05.

Joughin, 1., D.P. Winebrenner ant] M.A. Fahnestock. 1995. Observations of ice-sheet motion in Greenland using satellite radar interferometry. *Geophys. Res. Lett.*, 22(5), 571-574.

Joughin, 1., R. Kwok, M. Fahnestock, S, Gogineni and C. Allen. 1995. Interferometrically derived topography, velocity and ice-flux estimates for the Petermann Glacier. *EOS Trans.* Fall Meeting 1995. II 111)-09.

Kollmeyer, R.C. 1980, West Greenland outlet glaciers: An inventory of the major iceberg producers, in *World Glacier Inventory, Proceedings of the Workshop at Riederalp, Switzerland, 17-22 September 1978*, International Association of Hydrological Sciences, Publication No. 126, p. 57-65.

Rignot, E., **K**. Jezek and H.G. Sohn. 1995. Ice flow dynamics of the Greenland Ice Sheet from SAR Interferometry. *Geophys. Res. Lett.*, **22**(5), 575 578.

Rignot, E. 1995. Backscatter model for the unusual radar properties of the Greenland Ice Sheet, *J. Geophys. Res.* 100(1'; 5),9389-9400.

Rignot, E., K. Jezek and P. Gogineni. 1996. Tidal Motion, Ice Velocity and Ablation Rates of Petermann Gletscher from ERS-1 SAR Interferometry. *EOS Trans.* Spring Meeting 1996, T03.

Smith, A.M. 1991. The use of tiltmeters to study the dynamics of Antarctic ice-shelf grounding lines. *J. Glaciol.*, 37(125), 51- 58.

Vaughan, D.G. 1995. Tidal Flexure at ice shelf margins. *J. Geophys. Res.* 1 0 0 (1 1 4), 62136224.

Vaughan, D.G. and C.S.M. Doake. 1996. Recent atmospheric warming and retreat of ice shelves on the Antarctic peninsula. *Nature* 379, 328-331.

Zebker, H.A. and R.M. Goldstein. 1986. Topographic mapping from interferometric SAR observations. *J. Geophys. Res.*, **91** (B5), 4993 4999.

Zebker, H. A., P.A. Rosen, R.M. Goldstein, C. Werner and A. Gabriel. 1994. On the derivation of coseismic displacement fields using differential radar interferometry: the Landers Earthquake. *J. Geophys. Res.*, 99(1110), 19,61 7- 19,634.

Figure Captions

Fig. 1. ERS-1 SAR amplitude image of Petermann Gletscher acquired in February 1992. The white continuous line locates the tidal profile shown in Figure 5. The dotted white line represents the dynamic center-line of the glacier, which gives the ice flow direction. ©ESA 1992.

Fig. 2. Interferometric fringes for the image pair combining orbit 3205 and 3248, after removal of the interferometric baseline, and with a color intensity modulated by the phase coherence of the SAR signal. Dark areas are poorly correlated.

Fig. 3. Interferometrically-derived tidal flexure (color coded between 0 and 180 mm), and hinge-line (continuous white line) of Petermann Gletscher. The color intensity is modulated by the inverse of the radar brightness.

Fig. 4. Ice velocity of Petermann Gletscher, color coded between 0 and 1 20(I m a ', after correction is for the incidence angle of the radar illumination, flow direction, and tidal motion. The color intensity is modulate.d by the inverse of the radar brightness.

Fig. 5. Tidal displacements (dots) along the solid-line profile in Figure 1, compared to model predictions (solid-line) from an elastic beam theory. The longitudinal profile is 160 m wide or three SAR pixels per range line. The arrow points to the area of maximum bending stress, or hinge-line.

Fig. 6. Ice velocities along the glacier center-line after correction for an assumed flow direction. The dotted curve shows the ice velocities before tidal correction. The continuous curve shows ice velocities after removal of tidal flexure. The width of the longitudinal profile is 80 m.

Fig. 7. Ice discharge from Petermann Gletscher versus the along-flow distance from the hinge-line. The continuous curve was obtained by smoothing the results over GO range lines or 5 km. The dots show estimates obtained every range line or 80 m. The diamond symbol denotes ice discharge obtained by Higgins (1991) at the ice front.

Figure 1. Rignot, 1996.

Figure 2. Rignot, 1996.
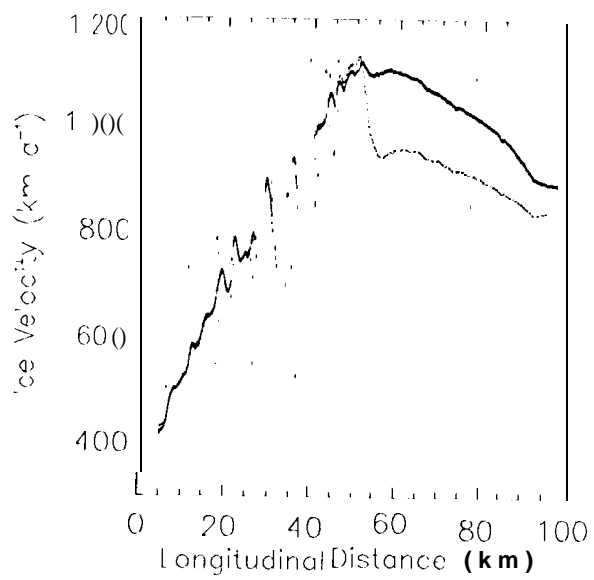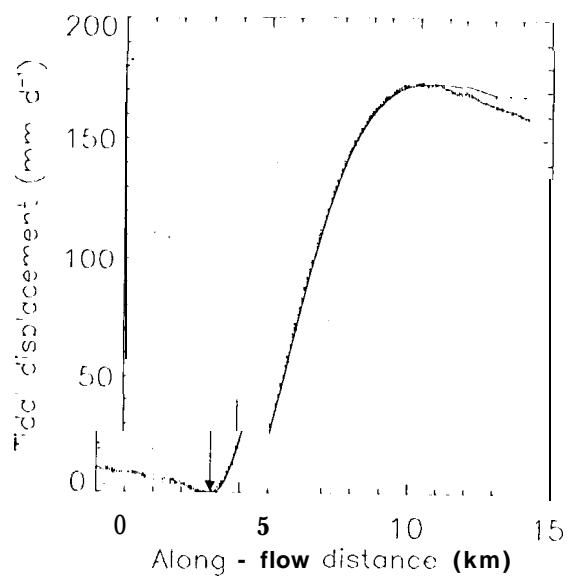
Figure 3. Rignot, 1996.

Figure 4. Rignot, 1996.
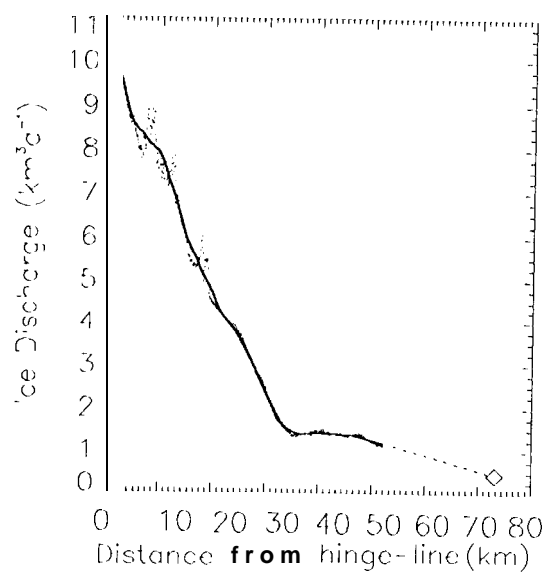
Figure 5. Rignot, 1996.

Figure 6. Rignot, **1996.**

Figure 7. Rignot, **1996.**